RESEARCH ARTICLE

Antibody responses to Zika virus proteins in pregnant and non-pregnant macaques

Anna S. Heffron[1☯], Emma L. Mohr[2☯], David Baker[1], Amelia K. Haj[1], Connor R. Buechler[1], Adam Bailey[1], Dawn M. Dudley[1], Christina M. Newman[1], Mariel S. Mohns[1], Michelle Koenig[1], Meghan E. Breitbach[1], Mustafa Rasheed[1], Laurel M. Stewart[1], Jens Eickhoff[3], Richard S. Pinapati[4], Erica Beckman[4], Hanying Li[4], Jigar Patel[4], John C. Tan[4], David H. O'Connor[1] *

1 Department of Pathology and Laboratory Medicine, University of Wisconsin-Madison, Madison, WI, United States of America, 2 Department of Pediatrics, School of Medicine and Public Health, University of Wisconsin-Madison, Madison, WI, United States of America, 3 Department of Biostatistics & Medical Informatics, University of Wisconsin-Madison, Madison, WI, United States of America, 4 Technology Innovation, Roche Sequencing Solutions, Madison, WI, United States of America

☯ These authors contributed equally to this work.
* dhoconno@wisc.edu

Abstract

The specificity of the antibody response against Zika virus (ZIKV) is not well-characterized. This is due, in part, to the antigenic similarity between ZIKV and closely related dengue virus (DENV) serotypes. Since these and other similar viruses co-circulate, are spread by the same mosquito species, and can cause similar acute clinical syndromes, it is difficult to disentangle ZIKV-specific antibody responses from responses to closely-related arboviruses in humans. Here we use high-density peptide microarrays to profile anti-ZIKV antibody reactivity in pregnant and non-pregnant macaque monkeys with known exposure histories and compare these results to reactivity following DENV infection. We also compare cross-reactive binding of ZIKV-immune sera to the full proteomes of 28 arboviruses. We independently confirm a purported ZIKV-specific IgG antibody response targeting ZIKV nonstructural protein 2B (NS2B) that was recently reported in ZIKV-infected people and we show that antibody reactivity in pregnant animals can be detected as late as 127 days post-infection (dpi). However, we also show that these responses wane over time, sometimes rapidly, and in one case the response was elicited following DENV infection in a previously ZIKV-exposed animal. These results suggest epidemiologic studies assessing seroprevalence of ZIKV immunity using linear epitope-based strategies will remain challenging to interpret due to susceptibility to false positive results. However, the method used here demonstrates the potential for rapid profiling of proteome-wide antibody responses to a myriad of neglected diseases simultaneously and may be especially useful for distinguishing antibody reactivity among closely related pathogens.

Author summary

ZIKV has emerged as a vector-borne pathogen capable of causing serious illness in infected adults and congenital birth defects. The vulnerability of communities to future ZIKV outbreaks will depend, in part, on the prevalence and longevity of protective immunity, thought to be mediated principally by antibodies. We currently lack diagnostic assays able to differentiate ZIKV-specific antibodies from antibodies produced following infection with closely related DENV, and we do not know how long anti-ZIKV responses are detectable. Here we profile antibodies recognizing linear epitopes throughout the entire ZIKV polyprotein, and we profile cross-reactivity with the proteomes of other co-endemic arboviruses. We show that while ZIKV-specific antibody binding can be detected, these responses are generally weak and ephemeral, and false positives may arise through DENV infection. This may complicate efforts to discern ZIKV infection and to determine ZIKV seroprevalence using linear epitope-based assays. The method used in this study, however, has promise as a tool for profiling antibody responses for a broad array of neglected tropical diseases and other pathogens and in distinguishing serology of closely-related viruses.

Introduction

Serologic assays designed to detect Zika virus (ZIKV) infection suffer from cross-reactivity with antibodies to closely related dengue virus (DENV), due to the high level of amino acid sequence identity (average ~55%) and structural similarity [1–4] between the two viruses. Humoral cross-reactivity with other similar arboviruses has been reported as well [1–2]. Serologic assays have been developed to detect past ZIKV infection, reporting sensitivity varying from 37% to 97% and specificity varying from 20% to 90% [5–8]. Most of these assays detect antibodies to the ZIKV envelope protein or nonstructural protein 1 (NS1) [7,9–11] and in one case, nonstructural protein 5 (NS5) [12]. A recent publication by Mishra et al. employed a high-density peptide microarray to identify antibodies to linear ZIKV epitopes lacking cross-reactivity with other flaviviruses [13]. This group identified an IgG immunoreactive peptide sequence in the ZIKV nonstructural protein 2B (NS2B) which induced little antibody binding in serum from ZIKV-naive people and was bound in early convalescence in most cases of symptomatic ZIKV infection [13]. This group did note seropositivity in a ZIKV-naive, DENV-immune individual and in one individual with no known flavivirus infection history.

Because ZIKV, DENV, and other arboviruses are similar in structure and acute clinical syndrome, are spread by the same mosquito vectors [14], and are co-endemic [15–16], it is difficult to identify people who have unequivocally been exposed to ZIKV only, adding uncertainty to efforts to profile ZIKV-specific antibody responses in humans. In contrast, macaques raised in indoor colonies can be infected specifically with ZIKV, DENV, or other pathogens. Macaque models of ZIKV infection provide a close approximation of human ZIKV infection in regards to natural history [17–20], tissue tropism [17–18,21–22], and transmission [18,23–26]. Importantly, macaques infected with ZIKV during pregnancy provide insight into the pathogenesis of congenital ZIKV infection [18–19,22–23,27–30]. Since the strain, dose, and timing of macaque model ZIKV infection is exactly known, the kinetics and specificity of humoral immune responses can be profiled in macaques with better resolution than is possible in cross-sectional human studies.

The peptide microarray technology we use in this study allows for one serum sample to be assayed against six million unique 16-residue peptides, or for 12 samples to each be assayed against 392,000 peptides, on a single chip (Roche Sequencing Solutions, Madison, WI). The

technology has been used in proteome-wide epitope mapping [31], profiling of antibody responses in autoimmune disease [32], profiling venom toxin epitopes [33], determining functions of cellular enzymes [34], *de novo* binding sequence discovery [35], epitope validation following phage display screening [36], and screening for tick-borne disease seroprevalence [37]. We previously used this tool to examine antibody responses in simian pegivirus (SPgV) and simian immunodeficiency virus (SIV) infections [38]. As mentioned above, a recent publication explored use of this technology in profiling human antibody responses against flaviviruses [13]. This linear peptide microarray technology has advantages over previous assays through its capacity to screen for reactivity to a large number of pathogens while simultaneously mapping reactive epitopes precisely, and it has the distinct advantage of allowing detection of unexpected epitopes due to its capacity to assay the entirety of a virus's proteome.

Here, we used high-density peptide microarrays to map macaque IgG epitopes in full-length ZIKV and DENV polyproteins and to compare cross-reactivity to 27 other arboviruses. Our study takes advantage of this technology's capacity to assess binding to linear epitopes throughout a virus' entire proteome to identify an epitope in ZIKV NS2B, a protein made intracellularly which embeds in the host cell's endoplasmic reticulum and thus would not be expected to induce strong antibody responses. We also demonstrate the potential of this technology, through its ability to survey binding throughout many whole viral proteomes simultaneously, to differentiate seroreactivity to an infecting virus from cross-reactivity against a great variety of other similar viruses. These unique aspects of this recently developed peptide microarray technology highlight its capacity to efficiently screen for and identify previously unknown epitopes in a large number of neglected disease-causing pathogens simultaneously and to distinguish infection histories of NTDs, potentially impacting the development of future diagnostics and vaccines.

Methods

Macaque study design

Animal demographics, inoculation strain, dose, and route, serum sample collection timelines, and array design used for each animal are described in Table 1. Gestational details and outcomes for pregnant animals are described in Table 2. Additional details on the study histories of the animals in this study can be found at https://go.wisc.edu/b726s1. All but one of the animals used in this study were born at the WNPRC indoor colonies. Animal H2 was born at the Caribbean Primate Research Center and tested negative for flavivirus exposure (specifically, for ZIKV and DENV exposure) using PRNTs prior to being admitted to the WNPRC colony.

Ethics

All monkeys were cared for by the staff at the Wisconsin National Primate Research Center (WNPRC) in accordance with the regulations and guidelines outlined in the Animal Welfare Act and the Guide for the Care and Use of Laboratory Animals and the recommendations of the Weatherall report (https://royalsociety.org/topics-policy/publications/2006/weatherall-report/). Per WNPRC standard operating procedures for animals assigned to protocols involving the experimental inoculation of an infectious pathogen, environmental enhancement included constant visual, auditory, and olfactory contact with conspecifics, the provision of feeding devices which inspire foraging behavior, the provision and rotation of novel manipulanda (e.g., Kong toys, nylabones, etc.), and enclosure furniture (i.e., perches, shelves). Per Animal Welfare Regulations (Title 9, Chapter 1, Subchapter A, Parts 1–4, Section 3.80 Primary enclosures) the animals were housed in a nonhuman primate Group 3 enclosure with at least 4.3 square feet of floor space and at least 30 inches of height. This study was approved by the

Table 1. Animal demographics.

Cohort	Animal	Public animal identifier*	Species	Sex	Flavivirus infection history	Inoculation strain	Inoculation dose and route	Time points of sample collection (days post infection, dpi)	Peptide array design
A	A1	cy0879	*Macaca fascicularis*	female	none	SIVmac239	7,000 TCID50, intrarectal	pre-infection, 125 dpi	Offset by 4, overlap of 12
	A2	cy0886	*Macaca fascicularis*	female	none	SIVmac239	7,000 TCID50, intrarectal	pre-infection, 126 dpi	Offset by 4, overlap of 12
B	B1	411359*	*Macaca mulatta*	female	none	Zika virus/H.sapiens-tc/FRA/2013/FrenchPolynesia-01_v1c1	10E4 PFU, subcutaneous	pre-infection, 28, 67 and 99 dpi	Offset by 1, overlap of 15
C	C1	295022*	*Macaca mulatta*	female	none	Zika virus/R.macaque-tc/UGA/1947/MR766-3329	10E4 PFU, subcutaneous	pre-infection, 28, 67 and 98 dpi	Offset by 1, overlap of 15
D	D1	448436*	*Macaca mulatta*	male	none	Zika virus/H.sapiens-tc/FRA/2013/FrenchPolynesia-01_v1c1	10E4 PFU, subcutaneous	pre-infection, 28 and 621 dpi	Offset by 1, overlap of 15
	D2	861138*	*Macaca mulatta*	female	none	Zika virus/H.sapiens-tc/FRA/2013/FrenchPolynesia-01_v1c1	10E4 PFU, subcutaneous	pre-infection, 28 and 582 dpi	Offset by 1, overlap of 15
F	F1	393422*	*Macaca mulatta*	male	Zika virus/H.sapiens-tc/FRA/2013/FrenchPolynesia-01_v1c1, 12 and 9.5 months prior	Dengue 2 New Guinea C	10E5 PFU, subcutaneous	pre-infection, 28 dpi	Offset by 4, overlap of 12
	F2	826226*	*Macaca mulatta*	male	Zika virus/H.sapiens-tc/FRA/2013/FrenchPolynesia-01_v1c1, 12 and 9.5 months prior	Dengue 2 New Guinea C	10E5 PFU, subcutaneous	pre-infection, 28 dpi	Offset by 4, overlap of 12
	F3	912116*	*Macaca mulatta*	male	Zika virus/H.sapiens-tc/FRA/2013/FrenchPolynesia-01_v1c1, 12 and 9.5 months prior	Dengue 2 New Guinea C	10E5 PFU, subcutaneous	pre-infection, 28 dpi	Offset by 4, overlap of 12
G	G1	660875*	*Macaca mulatta*	female	none	Zika virus/H.sapiens-tc/FRA/2013/FrenchPolynesia-01_v1c1	10E4 PFU, subcutaneous	pre-infection, 7, 21, 43, 78, 127 dpi	Offset by 1, overlap of 15
	G2	827577*	*Macaca mulatta*	female	none	Zika virus/H.sapiens-tc/FRA/2013/FrenchPolynesia-01_v1c1	10E4 PFU, subcutaneous	0, 7, 21, 35, 71, 113 days after primary infection	Offset by 4, overlap of 12
H	H1	146523*	*Macaca mulatta*	female	none	Zika virus/H.sapiens-tc/PUR/2015/PRVABC59	10E4 PFU, subcutaneous	pre-infection, 7, 21, 70 dpi	Offset by 1, overlap of 15
	H2	858972*	*Macaca mulatta*	female	none	Zika virus/H.sapiens-tc/PUR/2015/PRVABC59	10E4 PFU, subcutaneous	pre-infection, 7, 21, 70 dpi	Offset by 1, overlap of 15
	H3	419969*	*Macaca mulatta*	female	none	Zika virus/H.sapiens-tc/PUR/2015/PRVABC59	10E4 PFU, subcutaneous	pre-infection, 7, 21, 70 dpi	Offset by 1, overlap of 15
I	I1	776301*	*Macaca mulatta*	female	Dengue 3 Slenman/78, 9 months prior	Zika virus/H.sapiens-tc/PUR/2015/PRVABC59 bar code virus	10E4 PFU, subcutaneous	pre-infection, 8, 29, 57, 78 dpi	Offset by 4, overlap of 12

*Public animal identifiers are used in studies on the Zika Open Research Portal (https://zika.labkey.com/project/home/begin.view?).

Table 2. Gestational details.

Animal	Gestational days (gd) at inoculation	Pregnancy outcome
G1	36	delivery at 158 gd (122 dpi)
G2	38	delivery at 158 gd (120 dpi)
H1	46	fetectomy at 116 gd (70 dpi)
H2	47	fetectomy at 117 gd (70 dpi)
H3	43	fetectomy at 111 gd (68 dpi)
I1	35	delivery at 155 gd (120 dpi)

University of Wisconsin-Madison Graduate School Institutional Animal Care and Use Committee (animal protocol numbers G005401 and G005443).

Virus stocks

SIVmac239 (GenBank accession: M33262) stock was prepared by the WNPRC Virology Services Unit. Vero cells were transfected with the SIVmac239 plasmid. Infectious supernatant was then transferred onto rhesus PBMC. The stock was not passaged before collecting and freezing. ZIKV strain H/PF/2013 (GenBank accession: KJ776791) was obtained from Xavier de Lamballerie (European Virus Archive, Marseille, France) and passage history is described in Dudley et al. [17]. ZIKV strain MR766, ZIKV strain PRVABC59, and DENV-2 strain New Guinea C were generously provided by Brandy Russell (CDC, Ft. Collins, CO). ZIKV strain MR766 passage history has been described in Aliota et al. [39]. A molecularly-barcoded version of ZIKV strain PRVABC59 (Zika virus/H.sapiens-tc/PUR/2015/PRVABC59; GenBank accession: KU501215) was constructed as described in Aliota et al. [40]. DENV-2 strain New Guinea C (GenBank accession: FJ390389), originally isolated from a human in New Guinea, underwent 17 rounds of amplification on cells and/or suckling mice followed by a single round of amplification on C6/36 cells; virus stocks were prepared by inoculation onto a confluent monolayer of C6/36 mosquito cells. DENV-3 strain Sleman/78 was obtained from the NIH; virus stocks were prepared by a single passage on C6/36 cells.

Multiple sequence alignment

Full-length ZIKV and DENV polyprotein sequences were extracted from the National Center for Biotechnology Information (NCBI) database into Geneious Pro 9.1.8 (Biomatters, Ltd., Auckland, New Zealand). These sequences included the ZIKV and DENV polyprotein sequences described above (see "Virus stocks"), as well as DENV-1 strain VR-1254 (GenBank accession: EU848545) and DENV-4 strain VID-V2055 (GenBank accession: KF955510). These amino acid sequences were aligned using the Geneious alignment algorithm as implemented in Geneious Pro 9.1.8 using default parameters (global alignment with free end gaps, cost matrix: Blosum62).

Peptide array design and synthesis

Viral protein sequences were selected and submitted to Roche Sequencing Solutions (Madison, WI) for development into a peptide microarray as part of an early access program. Sequences included three ZIKV polyproteins (an Asian strain, ZIKV-FP, GenBank accession: KJ776791.2; an African strain, ZIKV-MR766, GenBank accession: KU720415.1; and an American strain, ZIKV-PR, GenBank accession: KU501215.1), four DENV polyproteins (DENV-1, GenBank accession: EU848545.1; DENV-2, GenBank accession: KM204118.1; DENV-3, GenBank accession: M93130.1; and DENV-4, GenBank accession: KF955510.1), and one SIVmac239 env

protein (GenBank accession: AAA47637.1), which were used for most analyses in this study. Sequences used for cumulative distribution function (CDF) plots (see Fig 3) and analysis include sequences for mosquito-borne viruses found in Africa and known to infect humans [41], as well as one Japanese encephalitis virus strain (GenBank accession: KX945367.1). Accession numbers used to represent each viral protein are listed in the supplemental material (S1 Table). Proteins were tiled as non-redundant 16 amino acid peptides, overlapping by 12 or 15 amino acids. The array designs are publicly available at https://go.wisc.edu/b726s1.

The peptide sequences were synthesized *in situ* with a Roche Sequencing Solutions Maskless Array Synthesizer (MAS) by light-directed solid-phase peptide synthesis using an amino-functionalized support (Geiner Bio-One) coupled with a 6-aminohexanoic acid linker and amino acid derivatives carrying a photosensitive 2-(2-nitrophenyl) propyloxycarbonyl (NPPOC) protection group (Orgentis Chemicals). Unique peptides were synthesized in random positions on the array to minimize impact of positional bias. Each array is comprised of twelve subarrays, where each subarray can process one sample and each subarray contains up to 392,318 unique peptide sequences.

Peptide array sample binding

Macaque serum samples were diluted 1:100 in binding buffer (0.01M Tris-Cl, pH 7.4, 1% alkali-soluble casein, 0.05% Tween-20). Diluted sample aliquots and binding buffer-only negative controls were bound to arrays overnight for 16–20 h at 4°C. After binding, the arrays were washed 3x in wash buffer (1x TBS, 0.05% Tween-20), 10 min per wash. Primary sample binding was detected via 8F1-biotin mouse anti-primate IgG (NIH Nonhuman Primate Reagent Resource) secondary antibody. The secondary antibody was diluted 1:10,000 (final concentration 0.1 ng/µl) in secondary binding buffer (1x TBS, 1% alkali-soluble casein, 0.05% Tween-20) and incubated with arrays for 3 h at room temperature, then washed 3x in wash buffer (10 min per wash) and 30 sec in reagent-grade water. The secondary antibody was labeled with Cy5-Streptavidin (GE Healthcare; 5 ng/µl in 0.5x TBS, 1% alkali-soluble casein, 0.05% Tween-20) for 1 h at room temperature, then the array was washed 2x for 1 min in 1x TBS, and washed once for 30 sec in reagent-grade water. Fluorescent signal of the secondary antibody was detected by scanning at 635 nm at 2 µm resolution and 25% gain, using an MS200 microarray scanner (Roche NimbleGen).

Peptide array data processing

The datafiles and analysis code for figures are available from https://go.wisc.edu/b726s1. A processed dataset is also available at this link to allow for greater ease in searching for specific sequences.

All figures in this analysis use the log base 2 of the raw fluorescence signal intensity values (measured using arbitrary units, A.U.). For each sample, each unique peptide was assayed and processed once; then results from peptides redundant to multiple proteomes (i.e. were present in more than one strain represented) were restored to each protein. Raw fluorescence intensity signal results from primary antibodies binding to peptides on the array, which have been labeled with a secondary antibody with a fluorescent tag. The amount of fluorescence signal is influenced by both the titer and affinity of primary antibodies binding to each peptide sequence.

For cumulative distribution function (CDF) plots, fluorescence signal intensities were log base 2 transformed and background reactivity in the blank (binding buffer only) control sample was subtracted for each peptide. The fold change from 0 dpi was calculated by subtracting reactivity at 0 dpi from reactivity at 28 dpi. To reduce instrument-related variance, the data was then filtered by taking the minimum intensity of two consecutive peptides with 1 amino

acid offset, thereby reducing peptide outliers by ensuring measured reactivity occurs in multiple consecutive peptides.

Validation of peptide array findings

To confirm the validity of our findings from this recently-developed peptide microarray platform, we assessed its performance against the humoral response produced by infection with simian immunodeficiency virus (SIV), which has been well-characterized by conventional methods such as enzyme-linked immunosorbent assays (ELISAs), enzyme-linked immunosorbent spot assays (ELISPOTs), epitope-prediction methods, or other protein arrays. We synthesized linear 16-mer peptides, overlapping by 12 amino acids, representing the SIVmac239 envelope protein (env) and analyzed serum from two Mauritian cynomolgus macaques for SIV-specific IgG reactivity before and approximately 125 days after SIVmac239 infection (Table 1). (We have previously plotted data procured from peptide array assays of these samples [38] while investigating the antibody response to SIV in the context of simian pegivirus infection; here we show the same data using the updated, improved data processing pipeline described above.) Post-infection samples showed fluorescence intensity as high as 1,000 times the intensity in pre-infection samples (S1 Fig). Regions of higher-fold increases in fluorescence intensity corresponded to previously defined variable domains of env which are known antibody targets, the variable loop regions, as well as others corresponding to known epitopes [42,43]. Taken together, these results validate epitope definition on the peptide microarray platform and show this platform to be capable of high-resolution virus-specific IgG epitope identification using the analytic methods utilized here.

Statistical analyses

Statistical analyses were performed using R (R Core Team 2018). Statistical significance of the change in signal intensity versus no change from pre-infection levels for each peptide was calculated using a two-tailed log-ratio t-test. For CDF plot analyses, statistical significance of the differences between virus species was determined using pooled t-tests.

Results

Identification of linear B cell epitopes in the ZIKV polyprotein

We sought to determine antibody binding, or reactivity, to the ZIKV polyprotein following ZIKV infection. We tiled 16-residue (16-mer) peptides overlapping by 15 amino acids representing different ZIKV polyproteins and evaluated the antibody binding of serum samples from animals with recent ZIKV-FP (animals B1, D1, and D2) or ZIKV-MR766 (animal C1) infections (Table 1). Animals in both groups had demonstrated neutralizing antibody responses at 28 dpi, measured by 90% plaque reduction neutralization tests (PRNT$_{90}$) as described previously [17,24,39]. Peptides were defined as reactive if the signal intensity was greater by any amount after infection with a cognate strain (e.g., increased signal intensity against ZIKV peptides in an animal infected with ZIKV) than it was before infection. Peptides were defined as cross-reactive if the signal intensity was greater by any amount after infection with a noncognate strain (e.g., increased signal intensity against ZIKV peptides in an animal infected with DENV). True epitopes were expected to induce reactivity greater than pre-infection reactivity by a statistically significant amount, and this statistical significance was expected to be seen in multiple overlapping peptides, since an antibody would be expected to bind multiple peptides with overlapping sequences. Statistical significance of the change in signal intensity versus no change was calculated using a two-tailed log-ratio t-test, and regions were only

considered epitopes when there was a statistically significant increase in intensity in a post-infection sample relative to intensity in a pre-infection sample in three or more consecutive peptides.

Reactivity was most commonly observed in three regions of the flavivirus polyprotein: envelope protein, NS2B, and nonstructural protein 3 (NS3). Therefore, most of the analysis in this paper is limited to these regions. Some antibody binding was seen in other regions of the polyprotein (for example, NS1, NS5), but this binding was scattered and inconsistent between animals (reactivity of all animals throughout the entire ZIKV polyprotein can be found in the supplemental material). Antibody binding to peptides from the envelope protein was seen in all four animals at 28 dpi; antibody binding in the NS3 region was seen in three out of four animals (Fig 1; reactivity throughout the entire ZIKV polyprotein can be seen in S2 Fig). The four animals exhibited similar responses against an Asian ZIKV strain, ZIKV-FP (Fig 1), as against an African strain and an American strain (ZIKV-MR766 and ZIKV-PR respectively, S3 Fig).

All four animals exhibited antibody binding to the ZIKV NS2B epitope similar to that documented in humans [13]. Though other reactive epitopes were identified in other proteins in multiple animals, this epitope was the only epitope in our study for which all ZIKV-infected animals showed reactivity. All ten ZIKV-infected animals in this study were used to determine statistical significance of this epitope in order to avoid making statistical inferences using very small sample sizes [44]. Area under the curve (AUC) values and corresponding receiver operating characteristic (ROC) curves were calculated (S4 Fig) to identify ten peptides at positions 1427–1436 in the polyprotein (for a total of 25 amino acids, sequence RAGDITWEK-DAEVTGNSPRLDVALD) as the best-performing epitope for which a statistically significant

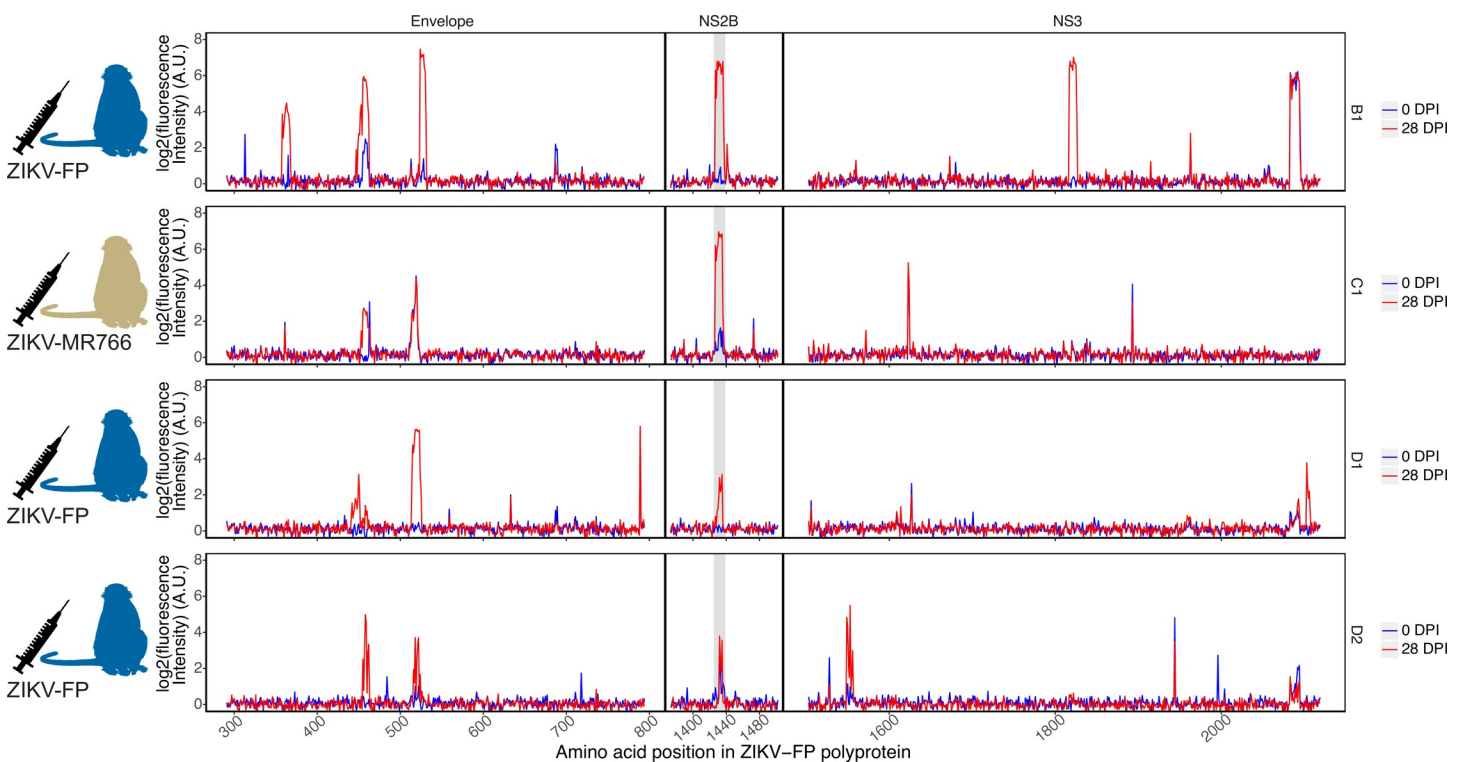**Fig 1. Reactivity of ZIKV-convalescent animals against the ZIKV-FP polyprotein.** Serum from rhesus macaques infected with ZIKV-FP (animals B1, D1, and D2) and with ZIKV-MR766 (animal C1) was assayed for IgG recognition of the ZIKV-FP polyprotein. Reactivity prior to infection and at 28 dpi is shown. The NS2B$_{1427-1451}$RD25 epitope is highlighted in grey.

https://doi.org/10.1371/journal.pntd.0006903.g001

change from 0 dpi was observed, hereafter referred to as NS2B$_{1427-1451}$RD25 (AUC of 0.9375, 95% confidence interval of 0.89065 to 0.9375). Using the mean signal intensity across the ten peptides, the change of signal intensity from 0 dpi to 21–28 dpi was statistically significant versus no change by a two-tailed log-ratio t-test (p-value = 0.000501 < 0.05, df = 9). This epitope is slightly longer than that found by Mishra et al. (nine 12-mer peptides, for a total of 20 amino acids, sequence DITWEKDAEVTGNSPRLDVA) [13].

Cross-reactivity of ZIKV-convalescent serum with DENV polyproteins and with arbovirus proteomes

DENV polyproteins share an average of 55% sequence identity with ZIKV polyproteins [1,2], and the region of DENV NS2B corresponding to the immunoreactive ZIKV NS2B$_{1427-1451}$RD25 epitope shares an average of 41% identity (Fig 2A). To examine cross-reactivity, we analyzed the antibody binding of samples from the ZIKV-convalescent animals against DENV polyproteins represented on the array (Fig 2B–2E). Cross-reactivity was apparent, with antibodies from the ZIKV-convalescent/DENV-naive animals recognizing regions of DENV
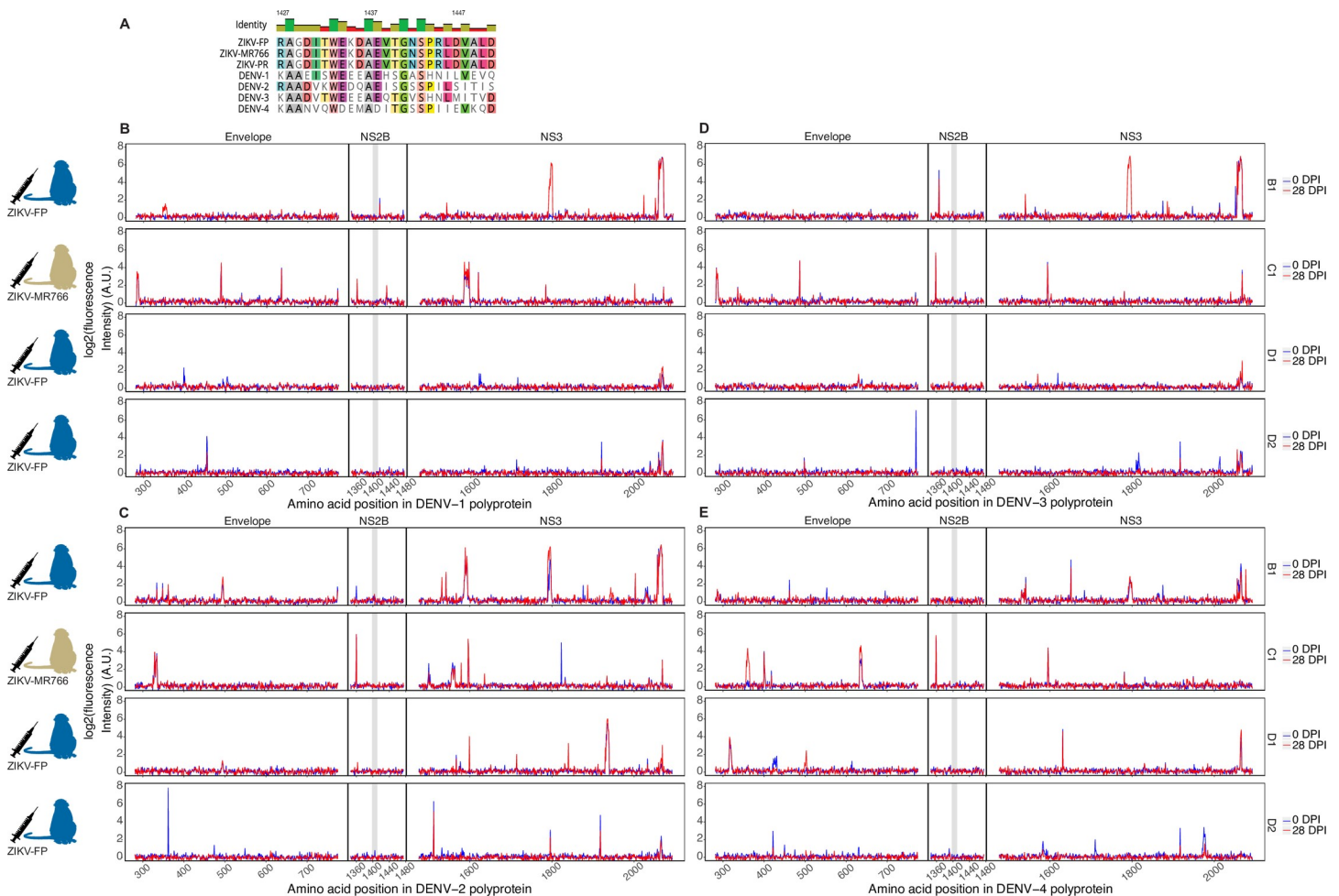
Fig 2. Cross-reactivity of ZIKV-convalescent animals against polyproteins of the four DENV serotypes. DENV serotypes share an average of 41% sequence similarity with the aligned ZIKV NS2B epitope (A). Serum from rhesus macaques infected with ZIKV-FP (animals B1, D1, and D2) or ZIKV-MR766 (C1) was assayed for cross-reactivity against polyproteins of DENV serotypes 1–4 (B-E, respectively). The segment of DENV NS2B which aligns with the ZIKV NS2B$_{1427-1451}$RD25 epitope is highlighted in grey.

https://doi.org/10.1371/journal.pntd.0006903.g002

polyproteins. All four animals showed some cross-reactivity against the DENV envelope protein and DENV NS3. Animals exhibited comparable cross-reactivities to all four DENV serotypes, with the highest single instance of cross-reactivity observed against a DENV-3 epitope in the NS3 region. No significant cross-reactivity against the DENV NS2B protein was observed for these or any ZIKV-infected animals in this study (p-value = 0.548, df = 9).

Given this array's capacity to screen for antibody binding to peptides representing many different virus proteomes at once, we also assessed cross-reactivity against the 27 other arboviruses (for a total of 28 arboviruses) represented. We plotted the fold change in reactivity from 0 to 28 dpi for each peptide in each virus's proteome using cumulative distribution function (CDF) plots (Fig 3). CDF plots were used to determine whether the sum of reactivity across a viral proteome could distinguish reactivity to the infecting pathogen (in this case, ZIKV) from cross-reactivity to a variety of other similar or dissimilar pathogens (in this case, 27 other arboviruses). Cross-reactivity in peptides in other arboviruses was observed, but it was rare compared with the reactivity seen in the ZIKV peptides. The greatest degree of cross-reactivity occurred among flaviviruses, in particular Ntaya virus, Spondweni virus, Bagaza virus, and DENV-3 (Fig 3C). Pooled t-tests showed significant differences between reactivity against ZIKV strains and other viruses for each of the four animals (Table 3). In animal B1, reactivity against ZIKV was significantly different from cross-reactivity against all other arboviruses (p-values ranging from <0.0001 to 0.0006). Animal C1's reactivity against ZIKV was significantly different (p-values <0.05) for all viruses assayed except Babanki virus, Banzi virus, DENV-4, Uganda S virus, and yellow fever virus. D1 showed reactivity against ZIKV that was significantly different from reactivity against all other viruses except Spondweni virus. D2 showed more significant cross-reactivity with other arboviruses; in D2, ZIKV reactivity differed significantly from reactivity to all other viruses except Bwamba virus, Chikungunya virus, DENV-1, Middelburg virus, Ndumu virus, Rift Valley fever virus, Spondweni virus, and Uganda S virus. Of note, D2 did also exhibit the smallest increase in fold change from 0 to 28 dpi in reactivity against ZIKV; this higher likelihood of cross-reactivity may be attributable to the minimal overall amount of reactivity present. Reactivity for the two ZIKV strains compared, one African strain (ZIKV-MR766, GenBank accession: NC_012532.1) and one Asian/American strain (GenBank accession: NC_035889.1) was not significantly different for any animal (p-values ranging from 0.62 to 0.88).

Anti-ZIKV antibody response during pregnancy

Given the importance of determining an accurate ZIKV infection history in pregnancy, we sought to characterize the gestational anti-ZIKV antibody response. We used the peptide microarray to evaluate serum samples from six pregnant animals. Animals were inoculated with ZIKV at 35–47 days post-conception (gestational date, gd) (Table 2). Two animals (G1 and G2) had no history of flavivirus exposure and were inoculated with ZIKV-FP at 36–38 gd. Three more flavivirus-naive animals (H1, H2, and H3) were infected with ZIKV-PR at 45–47 gd. One animal (I1) had a history of exposure to DENV-3 nine months prior to inoculation with a barcoded clone of ZIKV-PR at 35 gd [40]. Serum samples collected approximately one week post-infection and at two to six week intervals thereafter were analyzed against ZIKV polyproteins represented on the peptide array (Fig 4). All six pregnant animals exhibited anti-NS2B$_{1427-1451}$RD25 reactivity by the early convalescent phase (21–29 dpi), though time of initial appearance and duration of the response varied between animals.

All pregnant animals showed a similar pattern of anti-ZIKV reactivity, with some differences in time to peak reactivity and duration of detectable reactivity. In G1, elevated baseline intensity in the ZIKV NS2B$_{1427-1451}$RD25 region was present prior to inoculation with
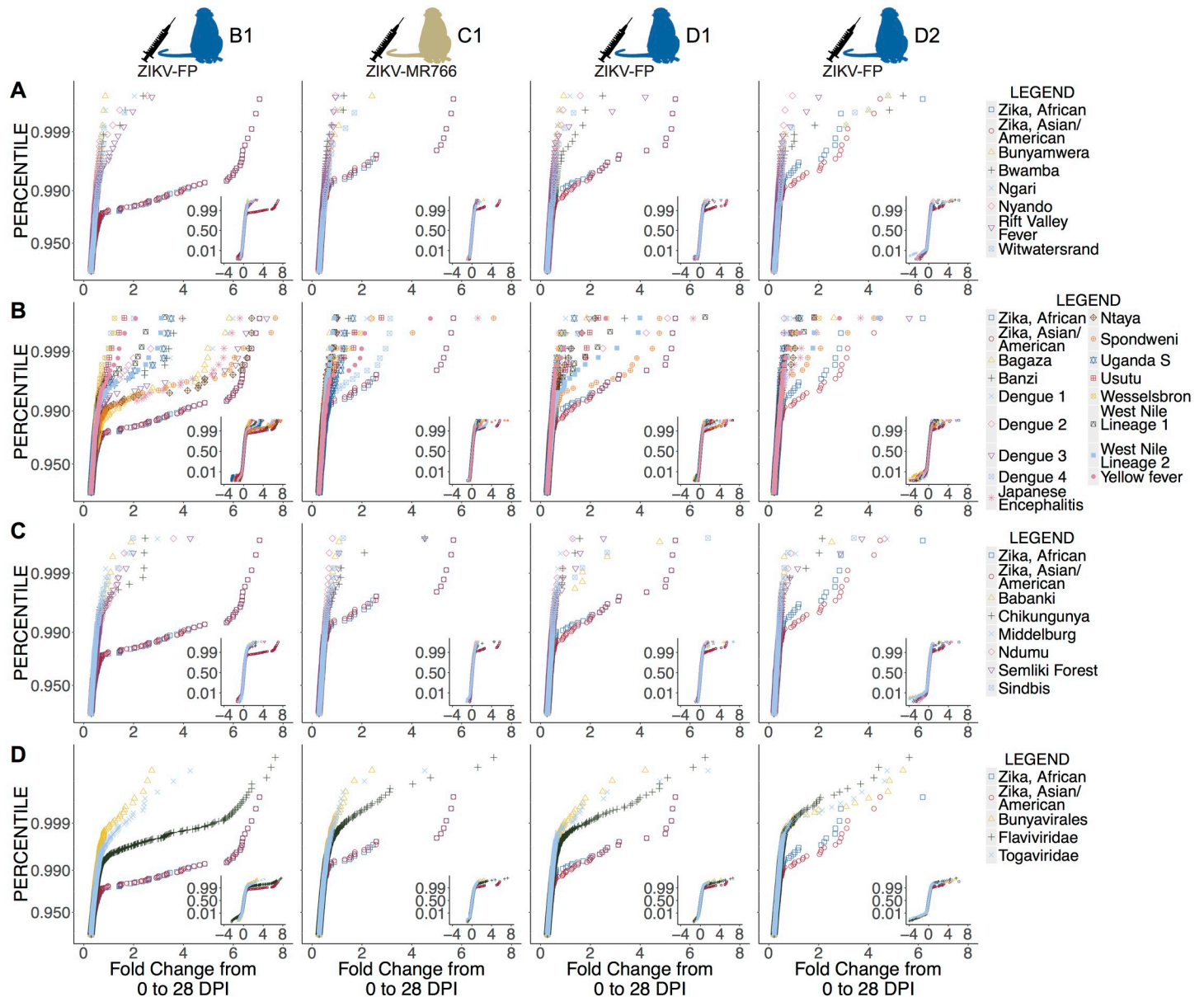
Fig 3. Cross-reactivity of sera from ZIKV-convalescent animals against the complete polyproteins or proteomes of 27 arboviruses represented on the array. Cumulative distribution function (CDF) plots of fold change from 0 dpi to 28 dpi of animals' reactivity and cross-reactivity to different viral proteomes are shown; data for animals infected with ZIKV-FP (B1, D1, and D2) and ZIKV-MR766 (C1) are shown. Reactivity to two ZIKV strains, one African and one Asian/American, is compared against all viruses on the array of order Bunyavirales (A), of family Togaviridae (B), of family Flaviviridae (C), and with the averages of reactivity of all viruses in Bunyavirales, of all viruses in Togaviridae, and of all viruses in Flaviviridae (D). The region of interest is shown large in the figure, while the full CDF plot is shown as an inset. ZIKV strains demonstrate significantly increased fold change in reactivity compared to the majority of other viruses represented on the array (see Table 3).

https://doi.org/10.1371/journal.pntd.0006903.g003

ZIKV-FP. Reactivity peaked in the acute phase (7 dpi) and subsequently decreased but remained above pre-infection levels through 127 dpi, after G1 had given birth. In G2, reactivity was not appreciable until the early convalescent phase (21 dpi) and peaked at 35 dpi, remaining elevated relative to pre-infection levels through the latest time point analyzed (113 dpi). Animals H1 and H3 showed elevated pre-infection intensity against NS2B$_{1427-1451}$RD25. All three animals in cohort H showed reactivity by 21 dpi. H1 and H2 continued to exhibit increased reactivity through the latest time point measured (70 dpi), while H3 had peak

Table 3. Significance of difference from ZIKV of summed reactivity.

Arbovirus family or order	Arbovirus species Arbovirus family or order	p-value for t-test against Asian/American ZIKV strain			
		B1	C1	D1	D2
Bunyavirales	Bunyamwera	<0.0001	0.0094	0.0001	0.0202
	Bwamba	<0.0001	0.0019	0.0030	0.2367*
	Ngari	<0.0001	0.0110	0.0015	0.0997*
	Nyando	<0.0001	0.0027	<0.0001	0.0001
	Rift Valley fever	<0.0001	0.0085	0.0001	0.1868*
	Witwatersrand	<0.0001	0.0083	0.0034	0.0289
Togaviridae	Babanki	<0.0001	0.0924*	0.0188	0.0004
	Chikungunya	<0.0001	0.0452	0.0002	0.0562*
	Middelburg	<0.0001	0.0081	0.0006	0.2074*
	Ndumu	<0.0001	0.0008	<0.0001	0.1681*
	Semliki Forest	<0.0001	0.0118	<0.0001	0.0053
	Sindbis	<0.0001	0.0417	0.0010	<0.0001
Flaviviridae	Bagaza	<0.0001	0.0010	0.0001	<0.0001
	Banzi	<0.0001	0.0609*	0.0060	0.0062
	Dengue 1	<0.0001	0.0010	0.0015	0.2522*
	Dengue 2	<0.0001	0.0006	0.0053	0.0074
	Dengue 3	0.0001	0.0067	0.0017	<0.0001
	Dengue 4	<0.0001	0.1880*	<0.0001	0.0038
	Japanese encephalitis	0.0002	0.0349	0.0045	0.0447
	Ntaya	0.0002	0.0002	<0.0001	0.0476
	Spondweni	0.0006	0.0015	0.5734*	0.2896*
	Uganda S	<0.0001	0.0608*	<0.0001	0.2134*
	Usutu	<0.0001	0.0129	0.0084	0.0053
	Wesselsbron	<0.0001	0.0032	0.0005	0.0002
	West Nile lineage 1	<0.0001	0.0007	0.0035	<0.0001
	West Nile lineage 2	<0.0001	0.0009	0.0052	0.0016
	Yellow fever	<0.0001	0.5379*	0.0003	0.0002
	Zika, African	0.7952*	0.6184*	0.8688*	0.7304*

*Non-significant values (p-value > 0.05).

https://doi.org/10.1371/journal.pntd.0006903.t003

reactivity at 21 dpi and decreased after. I1, an animal nine months post-DENV-3 infection, showed a pattern of reactivity similar to that in other animals, with anti-NS2B$_{1427-1451}$RD25 IgG reactivity first appearing at 8 dpi and peaking at 29 dpi at a level 3.6 times pre-infection reactivity (Fig 4). Reactivity remained close to peak reactivity through 78 dpi.

All pregnant animals' cross-reactivity against DENV polyproteins mirrored that seen in non-pregnant animals (S6 Fig). Binding of antibodies throughout the entire ZIKV-FP polyprotein can be found in the supplemental material (S7 Fig).

Differentiating DENV serology in ZIKV-immune animals

Previous assays have struggled to distinguish DENV serologic responses from ZIKV serologic responses [5–8]. We investigated whether the peptide microarray technology, and specifically reactivity patterns using the ZIKV NS2B$_{1427-1451}$RD25 epitope, could distinguish DENV from ZIKV infections. Three animals (cohort F) had been challenged twice with ZIKV-FP 12 months prior and 9.5 months prior [17]; we collected serum from these animals, infected them with DENV-2, and collected serum 28 days after. These samples were analyzed against 16-mer
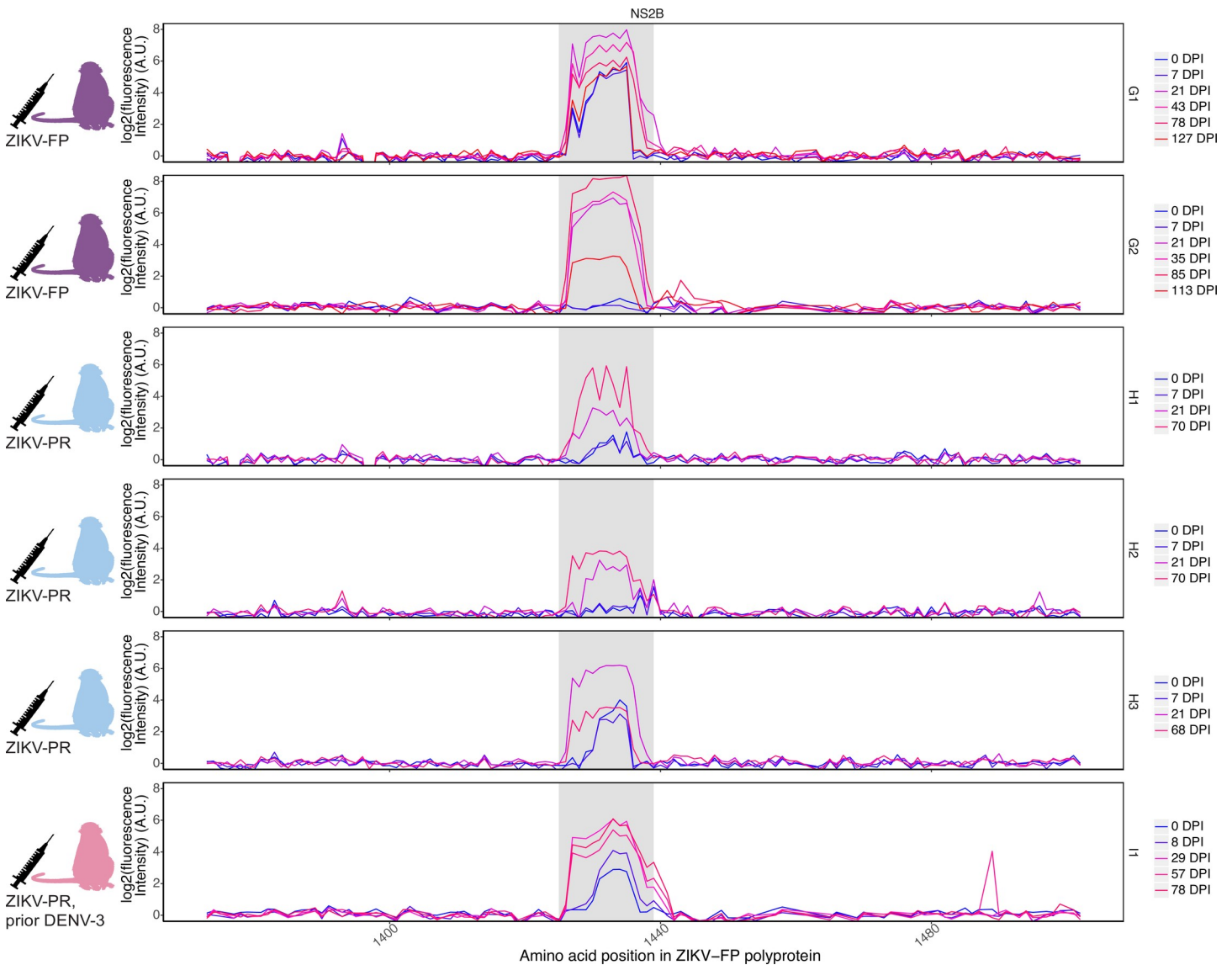
Fig 4. IgG reactivity against ZIKV NS2B$_{1427-1451}$RD25 during pregnancy. Serum samples taken throughout the course of six animals' pregnancies were evaluated against the ZIKV-FP polyprotein represented on peptide microarrays. Two animals (G1 and G2) were infected with ZIKV-FP at 36–38 gd. Three animals (H1, H2, H3) were infected with ZIKV-PR at 45–47 gd. One animal (I1) had been infected with DENV-3 nine months prior and was infected with a barcoded clone of ZIKV-PR at 35 gd. The NS2B$_{1427-1451}$RD25 epitope is highlighted in grey. Reactivity against the ZIKV-FP envelope and NS3 proteins can be found in S5 Fig.

https://doi.org/10.1371/journal.pntd.0006903.g004

peptides, with amino acid overlap of 12, representing DENV-2 and ZIKV-FP (Fig 5). Binding of antibodies throughout the entire DENV-2 and ZIKV-FP polyproteins can be found in the supplemental material (S8 Fig).

These animals showed reactivity against all four DENV polyproteins in regions representing the DENV envelope protein, DENV NS3, and others (Fig 5A) and cross-reactivity against corresponding regions of the ZIKV polyprotein (Fig 5B). One animal (F3) out of the three showed significant reactivity to the NS2B$_{1427-1451}$RD25 epitope, though this reactivity was slightly outside the area of typical NS2B$_{1427-1451}$RD25 reactivity (peptides 1421–1444 rather than 1427–1451). Another (F1) showed elevated pre-DENV infection intensity in NS2B$_{1427-1451}$RD25 that did not change following DENV infection, possibly as a result of the animal's
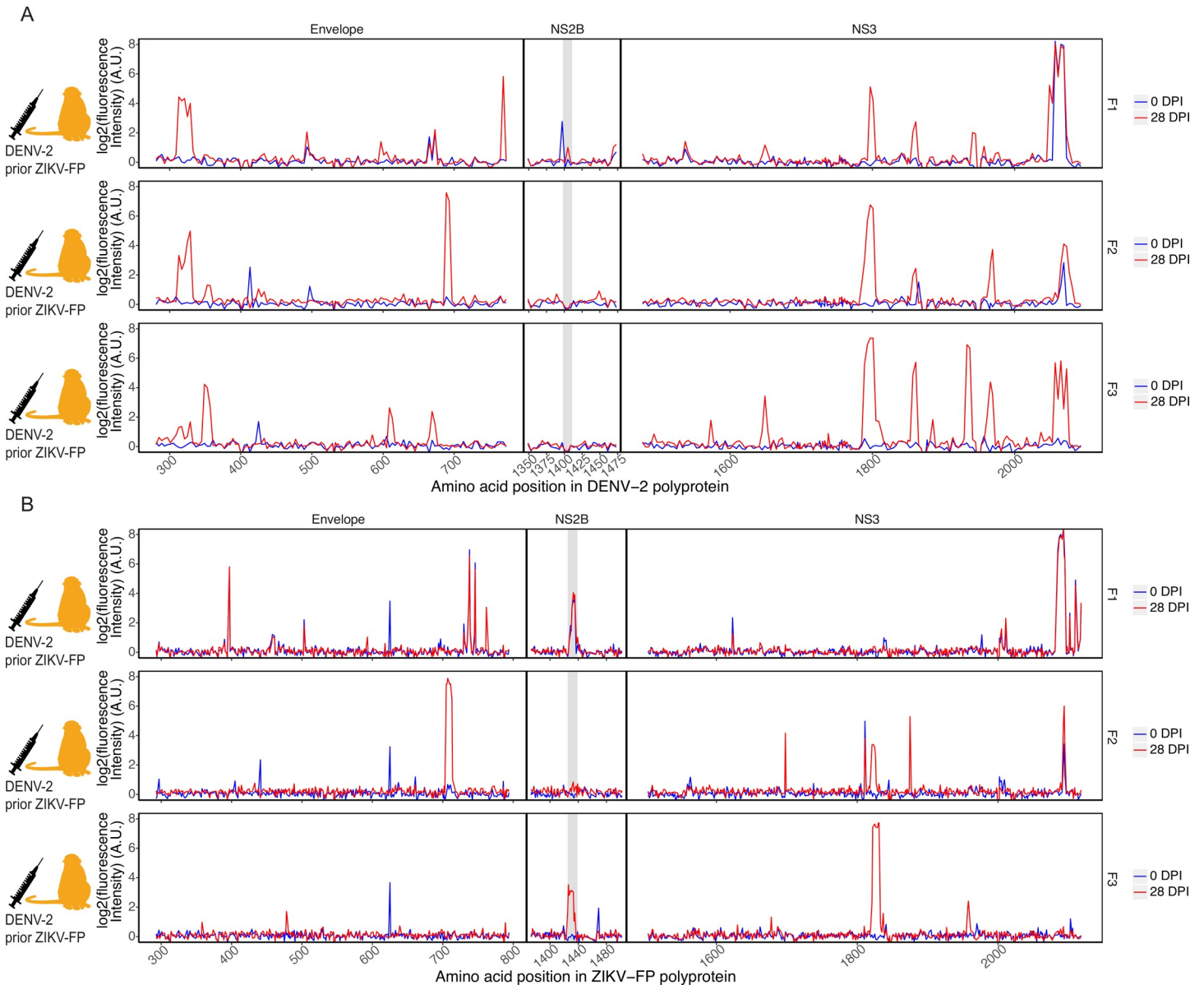
Fig 5. Antibody reactivity to DENV and ZIKV polyproteins of animals with recent DENV infection. Three macaques (F1, F2, and F3), with history of challenge and rechallenge with ZIKV-FP 12 and 9.5 months prior, were infected with DENV-2 and serum samples taken before DENV infection and at 28 dpi were assessed. Reactivity of these animals against peptides representing the envelope, NS2B, and NS3 proteins of DENV-2 (A) and ZIKV-FP (B) is shown. The ZIKV NS2B$_{1427-1451}$RD25 epitope (in B) is highlighted in grey; the corresponding region in the DENV NS2B protein is likewise highlighted (in A).

prior ZIKV exposure. Animal F2 showed no detectable NS2B$_{1427-1451}$RD25 reactivity before or after exposure.

Discussion

We describe the antibody binding of the anti-ZIKV IgG response in non-pregnant and pregnant rhesus macaques and compare this to the anti-DENV response. Using a recently developed high-density peptide microarray we show that macaques infected with ZIKV produce IgG antibodies which bind throughout the ZIKV polyprotein, including conserved antibody

binding to an epitope in ZIKV NS2B, NS2B$_{1427-1451}$RD25, which is apparent regardless of the ZIKV strain used for infection. We establish that cross-reactivity exists between anti-ZIKV and anti-DENV antibodies for the ZIKV and DENV polyproteins, and we show this technology can be used to differentiate anti-ZIKV reactivity from cross-reactivity to many other arboviruses. Additionally, we show the anti-NS2B$_{1427-1451}$RD25 IgG response is susceptible to false positives in the context of DENV infection and may be susceptible to false-positives in flavivirus-immune individuals. Thus, while this epitope may be broadly useful for serosurveillance, it should be used with caution in the diagnosis of individual infections.

As has been seen in previous assays [2,10,12–13,45–48], we observed antibody cross-reactivity between ZIKV- and DENV-immune sera, though reactivity to the ZIKV NS2B$_{1427-1451}$RD25 epitope was observed in all cases of recent ZIKV infection (10 out of 10 ZIKV-infected animals), and in only one out of three cases of recent DENV infection in animals with history of ZIKV exposure. Reactivity to the NS2B epitope was conserved whether the infecting strain was African, Asian, or American in origin. All ZIKV-infected animals produced anti-ZIKV IgG against the NS2B$_{1427-1451}$RD25 epitope, though reactivity was sometimes small in magnitude (as in animal D2) or was measurable for only a short duration (as in animal H3). The lack of uniformity of the anti-ZIKV IgG response is especially relevant since all ZIKV-exposed animals could be followed, in contrast to studies in humans where there may be a selection bias for individuals with symptomatic ZIKV, which is thought to account for only approximately half of ZIKV infections [13,49]. Though anti-NS2B$_{1427-1451}$RD25 reactivity was consistently detectable in early convalescence, it decayed in all but one case, that of a pregnant animal with previous DENV exposure, during the time period assessed. These findings corroborate findings in humans, in which symptomatic ZIKV infection was strongly associated with detectable anti-NS2B antibodies in the early convalescent phase (96%), but was less likely six months post-infection (44%) [13]. These results demonstrate the need for further investigation into the longevity and kinetics of the anti-ZIKV humoral response. Given that no other purported ZIKV-specific epitopes have been identified to date, these results also call into question how useful current serological methods may be in differentiating past ZIKV exposure from exposure to other flaviviruses. Additionally, one animal (F3) with a history of previous ZIKV infections showed reactivity against the ZIKV NS2B$_{1427-1451}$RD25 epitope following experimental DENV infection, indicating that a history of ZIKV infection or a recent DENV infection has potential to confound results using this epitope. Thus, while this epitope appears to be more ZIKV-specific than most, its utility in guiding development of diagnostics will likely be limited.

The ability of the peptide array to differentiate seroreactivity against ZIKV from cross-reactivity to other viruses and to show cross-reactivity to 27 other mosquito-borne arboviruses suggests this technology, with additional optimization, could be useful for determining the etiology of fever of unknown origin and other non-specific symptoms in areas where mosquito-borne diseases are common. All ZIKV-infected animals showed the greatest fold change from 0 dpi (equal to the log2 differences from 0 dpi) in reactivity against ZIKV proteomes. Though these differences in fold change did not always reach significance for all strains in all animals, the tendency to show the greatest reactivity in ZIKV strains, even in comparisons against very closely-related flaviviruses, for ZIKV-infected animals demonstrates the potential of this technology in guiding diagnostic development in the future.

This assay detected anti-NS2B$_{1427-1451}$RD25 reactivity in all pregnant macaques exposed to ZIKV. Production of IgG antibodies has relevance to both mother and fetus, since maternal IgG crosses the placenta and transport of IgG across the placental barrier increases throughout the course of pregnancy [50]. It can be presumed the anti-ZIKV IgG produced by these animals also reached their fetuses, but whether these anti- NS2B$_{1427-1451}$RD25 antibodies provide protection, contribute to the pathogenesis of ZIKV disease and ZIKV congenital effects, or are

irrelevant in ZIKV pathology is currently unknown. Though we did not note any variation in outcomes with differences in antibody responses, it is possible deviations in antibody responses during pregnancy could help explain differences in outcomes following gestational ZIKV infection. Several pregnant animals also showed elevated pre-infection intensity at the $NS2B_{1427-1451}RD25$ epitope. This phenomenon may be due to innate immunodominance of the $NS2B_{1427-1451}RD25$ epitope, or it may be due to molecular mimicry, though we have not found this epitope present in any other pathogen. These findings merit further and more thorough investigation than this current study can provide.

The peptide array technology used in this study has several limitations. The assay's utility could be increased by the addition of quantitative capacities. We currently use a 1:100 antibody dilution since we have found this to produce an optimal signal:noise ratio, but it is possible serial dilutions could allow for measurement of quantitative results. Greater confidence in this assay's results could be derived from assessing its ability to identify the binding of well-characterized monoclonal antibodies. Once validated in this way, the array could then be used to determine the specificity of new monoclonal antibodies as they are discovered. Additionally, our study defined a positive response as an increase from an animal's pre-infection intensity; human patients usually cannot give pre-infection samples and must rely upon controls determined from humans having no known history of exposure to certain pathogens. The development of such a control would raise the specificity of the assay at the expense of sensitivity, and thus would risk missing some true positive results when definitive pre-infection samples from the same individual are not available.

The peptide array approach is also limited due to its reliance on continuous linear epitopes. Many previously documented ZIKV epitopes are discontinuous conformational epitopes [51–57]. It is also possible that this array may miss some immunodominant responses or other clinically important immune responses. For example, antibody binding to the NS1 protein has been observed and is frequently described in other studies [7,9–11], but binding to NS1 was scattered and inconsistent using the peptide microarrays. Other epitope discovery methods will likely remain superior in defining discontinuous conformational epitopes and immunodominant responses, but this technology is useful in identifying immunoreactive regions not previously considered as potential epitopes. Given that conformational epitopes are often cross-reactive between flaviviruses [52,58] this assay's ability to detect only linear epitopes may make it more beneficial in diagnostic development. Past work from our laboratory, including results from some of the animals whose sera was analyzed here, has shown anti-ZIKV neutralizing antibody titers measured by $PRNT_{90}$ do not drop off but remain elevated as late as 64 dpi [17]. The discordance between levels of anti-$NS2B_{1427-1451}RD25$ IgG and neutralizing antibody titers may indicate the anti-$NS2B_{1427-1451}RD25$ antibodies do not play a role in protection against future infections, which may explain the drop-off observed in macaques and in humans.

In the future, this technology could be expanded for use in profiling antibody responses to many other pathogens. This tool was able to detect known and previously unknown epitopes throughout the ZIKV proteome, including epitopes in unexpected regions such as NS2B. This approach could be applied to other NTDs to advance diagnostic and vaccine development. The array used in this study simultaneously evaluates antibody responses against the entire proteomes of every mosquito-borne virus known to infect humans in Africa. Building off what we have learned through this and other peptide array analyses, we intend to use this array to survey antibody reactivity in African populations, through which we may identify previously unknown epitopes for some of the rare pathogens represented on the array. Additionally, we plan to use this assay to evaluate and compare both IgM and IgG responses in these analyses, which may help elucidate the kinetics of the immediate and long-term antibody response to pathogens.

In summary, this work in macaques demonstrates the capacity of a recently developed peptide microarray to profile the binding of distinct anti-ZIKV and anti-DENV IgG antibody responses in experimental infections. Our work shows the anti-NS2B$_{1427\text{-}1451}$RD25 IgG response is characterized by relatively rapid decay and is susceptible to confounding, mirroring results seen in humans. The peptide microarray technology used shows particular promise in evaluating full-proteome antibody binding for a large number of pathogens efficiently and may be especially useful for neglected tropical diseases for which diagnostics are rudimentary or non-existent.

Supporting information

S1 Table. Arboviral proteins and polyproteins used for CDF plot analysis.
(TIF)

S1 Fig. SIV env epitopes identified by a high-density peptide microarray overlap known epitopes in variable loop regions. Serum from two Mauritian cynomolgus macaques (animals A1 and A2) before and after infection with SIVmac239 env was evaluated for reactivity to overlapping peptides representing the SIVmac239 env protein sequence on a linear peptide microarray. SIV env variable loop regions [41] are highlighted in grey.
(TIF)

S2 Fig. Reactivity of B1, C1, D1, and D2 against the complete polyprotein of ZIKV-FP. The NS2B$_{1427\text{-}1451}$RD25 epitope is highlighted in grey.
(TIF)

S3 Fig. Reactivity of B1, C1, D1, and D2 against ZIKV-MR766 (A) and ZIKV-PR (B). The NS2B1427-1451RD25 epitope is highlighted in grey.
(TIF)

S4 Fig. ROC curves for best-performing epitope and multidimensional scaling (MDS) plot for different time points. ROC curves (A) were generated using data from the 8 animals analyzed against ZIKV polyproteins tiled as 16 amino acid peptides overlapping by 15 amino acids since this was the most complete dataset. ROC curves were created using the 8 samples collected at 0 DPI as the control group and the same 8 samples collected at 21–28 DPI samples as the test group. We chose consecutive peptides within the NS2B region that maximized the differences of mean log-normalized intensities between the controls and test samples. The decision threshold was determined by maximizing the AUC and the resulting ROCs of 9 to 13 peptides were plotted. ROC curves overlapped. MDS plots (B) of distances between the log-normalized gene expression profiles were created using Limma plot MDS R library. Only the 10 peptides in the identified NS2B$_{1427\text{-}1451}$RD25 epitope were used. Based on MDS analysis, pre-infection samples (blue), samples from early convalescence (21–28 dpi, red), and samples from any later time (>43 dpi, yellow) clustered in separate groups.
(TIF)

S5 Fig. Reactivity of cohort G (ZIKV-FP infection during first trimester), H (ZIKV-PR infection during first trimester), and I (history of DENV-3 infection, ZIKV-PR infection during first trimester) against the ZIKV-FP polyprotein. The NS2B$_{1427\text{-}1451}$RD25 epitope is highlighted in grey.
(TIF)

S6 Fig. Reactivity of cohort G (ZIKV-FP infection during first trimester), H (ZIKV-PR infection during first trimester), and I (history of DENV-3 infection, ZIKV-PR infection during first trimester) against the DENV-2 polyprotein. The region of the DENV-2

polyprotein corresponding to the ZIKV NS2B$_{1427-1451}$RD25 epitope is highlighted in grey.
(TIF)

S7 Fig. Reactivity of cohorts G, H, and I against the complete polyprotein of ZIKV-FP. The NS2B$_{1427-1451}$RD25 epitope is highlighted in grey.
(TIF)

S8 Fig. Reactivity of cohort F against the complete polyproteins of ZIKV-FP (A) and DENV-2 (B). The NS2B1427-1451RD25 epitope in ZIKV-FP, and the corresponding area in DENV-2, is highlighted in grey.
(TIF)

Acknowledgments

Author Contributions

Conceptualization: Anna S. Heffron, Emma L. Mohr, Connor R. Buechler, Adam Bailey, Dawn M. Dudley, Christina M. Newman, Jigar Patel, John C. Tan, David H. O'Connor.

Data curation: Anna S. Heffron, David Baker, Amelia K. Haj, Adam Bailey, Richard S. Pinapati, John C. Tan, David H. O'Connor.

Formal analysis: Anna S. Heffron, David Baker, Amelia K. Haj, Jens Eickhoff, Jigar Patel, John C. Tan, David H. O'Connor.

Funding acquisition: David H. O'Connor.

Investigation: Anna S. Heffron, Emma L. Mohr, David Baker, Amelia K. Haj, Connor R. Buechler, Adam Bailey, Dawn M. Dudley, Christina M. Newman, Mariel S. Mohns, Michelle Koenig, Meghan E. Breitbach, Mustafa Rasheed, Laurel M. Stewart, Richard S. Pinapati, Erica Beckman, Hanying Li, John C. Tan, David H. O'Connor.

Methodology: Anna S. Heffron, Emma L. Mohr, David Baker, Jens Eickhoff, Richard S. Pinapati, John C. Tan, David H. O'Connor.

Project administration: Anna S. Heffron, Emma L. Mohr, Dawn M. Dudley, Christina M. Newman, John C. Tan, David H. O'Connor.

Resources: Anna S. Heffron, Emma L. Mohr, Connor R. Buechler, Dawn M. Dudley, Christina M. Newman, Mariel S. Mohns, Michelle Koenig, Meghan E. Breitbach, Mustafa Rasheed, Laurel M. Stewart, Erica Beckman, Hanying Li, David H. O'Connor.

Software: Anna S. Heffron, David Baker, Amelia K. Haj, David H. O'Connor.

Supervision: Anna S. Heffron, Emma L. Mohr, John C. Tan, David H. O'Connor.

Validation: Anna S. Heffron, Emma L. Mohr, David Baker, Hanying Li, David H. O'Connor.

Visualization: Anna S. Heffron, Emma L. Mohr, David Baker, Amelia K. Haj, Jens Eickhoff, David H. O'Connor.

Writing – original draft: Anna S. Heffron, Emma L. Mohr, John C. Tan.

Writing – review & editing: Anna S. Heffron, Emma L. Mohr, David Baker, Amelia K. Haj, Adam Bailey, Dawn M. Dudley, Christina M. Newman, Mariel S. Mohns, Meghan E. Breitbach, Mustafa Rasheed, Jens Eickhoff, John C. Tan, David H. O'Connor.

References

1. Chang HH, Huber RG, Bond PJ, Grad YH, Camerini D, Maurer-Stroh S et al. Systematic analysis of protein identity between Zika virus and other arthropod-borne viruses. Bull World Health Organ. 2017; 95:517–525I. https://doi.org/10.2471/BLT.16.182105 PMID: 28670016

2. Xu X, Vaughan K, Weiskopf D, Grifoni A, Diamond MS, Sette A et al. Identifying Candidate Targets of Immune Responses in Zika Virus Based on Homology to Epitopes in Other Flavivirus Species. PLoS Curr. 2016; 8

3. Xu X, Song H, Qi J, Liu Y, Wang H, Su C et al. Contribution of intertwined loop to membrane association revealed by Zika virus full-length NS1 structure. EMBO J. 2016; 35:2170–2178. https://doi.org/10.15252/embj.201695290 PMID: 27578809

4. Harrison SC. Immunogenic cross-talk between dengue and Zika viruses. Nat Immunol. 2016; 17:1010–1012. https://doi.org/10.1038/ni.3539 PMID: 27540984

5. Safronetz D, Sloan A, Stein DR, Mendoza E, Barairo N, Ranadheera C et al. Evaluation of 5 Commercially Available Zika Virus Immunoassays. Emerg Infect Dis. 2017; 23:1577–1580. https://doi.org/10.3201/eid2309.162043 PMID: 28665268

6. Wong SJ, Furuya A, Zou J, Xie X, Dupus AP 2nd, Kramer LD et al. A Multiplex Microsphere Immunoassay for Zika Virus Diagnosis. EBioMedicine. 2017; 16:136–140. https://doi.org/10.1016/j.ebiom.2017.01.008 PMID: 28094237

7. Granger D, Hilgart H, Misner L, Christensen J, Bistodeau S, Palm J et al. Serologic Testing for Zika Virus: Comparison of Three Zika Virus IgM-Screening Enzyme-Linked Immunosorbent Assays and Initial Laboratory Experiences. J Clin Microbiol. 2017; 55:2127–2136. https://doi.org/10.1128/JCM.00580-17 PMID: 28446573

8. Goncalves A, Peeling RW, Chu MC, Gubler DJ, de Silva AM, Harris E et al. Innovative and New Approaches to Laboratory Diagnosis of Zika and Dengue: A Meeting Report. J Infect Dis. 2018; 217:1060–1068. https://doi.org/10.1093/infdis/jix678 PMID: 29294035

9. Lee AJ, Bhattacharya R, Scheuermann RH, Pickett BE. Identification of diagnostic peptide regions that distinguish Zika virus from related mosquito-borne Flaviviruses. PLoS One. 2017; 12:e0178199. https://doi.org/10.1371/journal.pone.0178199 PMID: 28562637

10. Balmaseda A, Stettler K, Medialdea-Carrera R, Collado D, Jin X, Zambrana JV et al. Antibody-based assay discriminates Zika virus infection from other flaviviruses. Proc Natl Acad Sci U S A. 2017; 114:8384–8389. https://doi.org/10.1073/pnas.1704984114 PMID: 28716913

11. L'Huillier AG, Hamid-Allie A, Kristjanson E, Papageorgiou L, Hung S, Wong CF et al. Evaluation of Euroimmun Anti-Zika Virus IgM and IgG Enzyme-Linked Immunosorbent Assays for Zika Virus Serologic Testing. J Clin Microbiol. 2017; 55:2462–2471. https://doi.org/10.1128/JCM.00442-17 PMID: 28566316

12. Shan C, Ortiz DA, Yang Y, Wong SJ, Kramer LD, Shi PY et al. Evaluation of a Novel Reporter Virus Neutralization Test for Serological Diagnosis of Zika and Dengue Virus Infection. J Clin Microbiol. 2017; 55:3028–3036. https://doi.org/10.1128/JCM.00975-17 PMID: 28768729

13. Mishra N, Caciula A, Price A, Thakkar R, Ng J, Chauhan LV et al. Diagnosis of Zika Virus Infection by Peptide Array and Enzyme-Linked Immunosorbent Assay. MBio. 2018; 9

14. Paixão ES, Teixeira MG, Rodrigues LC. Zika, chikungunya and dengue: the causes and threats of new and re-emerging arboviral diseases. BMJ Glob Health. 2018; 3:e000530. https://doi.org/10.1136/bmjgh-2017-000530 PMID: 29435366

15. Carrillo-Hernández MY, Ruiz-Saenz J, Villamizar LJ, Gómez-Rangel SY, Martínez-Gutierrez M. Co-circulation and simultaneous co-infection of dengue, chikungunya, and zika viruses in patients with febrile syndrome at the Colombian-Venezuelan border. BMC Infect Dis. 2018; 18:61. https://doi.org/10.1186/s12879-018-2976-1 PMID: 29382300

16. Azeredo EL, Dos Santos FB, Barbosa LS, Souza TMA, Badolato-Corrêa J, Sánchez-Arcilla JC et al. Clinical and Laboratory Profile of Zika and Dengue Infected Patients: Lessons Learned From the Co-circulation of Dengue, Zika and Chikungunya in Brazil. PLoS Curr. 2018; 10

17. Dudley DM, Aliota MT, Mohr EL, Weiler AM, Lehrer-Brey G, Weisgrau KL et al. A rhesus macaque model of Asian-lineage Zika virus infection. Nat Commun. 2016; 7:12204. https://doi.org/10.1038/ncomms12204 PMID: 27352279

18. Nguyen SM, Antony KM, Dudley DM, Kohn S, Simmons HA, Wolfe B et al. Highly efficient maternal-fetal Zika virus transmission in pregnant rhesus macaques. PLoS Pathog. 2017; 13:e1006378.

19. Martinot AJ, Abbink P, Afacan O, Prohl AK, Bronson R, Hecht JL et al. Fetal Neuropathology in Zika Virus-Infected Pregnant Female Rhesus Monkeys. Cell. 2018; 173:1111–1122.e10. https://doi.org/10.1016/j.cell.2018.03.019 PMID: 29606355

20. Osuna CE, Lim SY, Deleage C, Griffin BD, Stein D, Schroeder LT et al. Zika viral dynamics and shedding in rhesus and cynomolgus macaques. Nat Med. 2016; 22:1448–1455. https://doi.org/10.1038/nm.4206 PMID: 27694931

21. Hirsch AJ, Smith JL, Haese NN, Broeckel RM, Parkins CJ, Kreklywich C et al. Zika Virus infection of rhesus macaques leads to viral persistence in multiple tissues. PLoS Pathog. 2017; 13:e1006219.

22. Hirsch AJ, Roberts VHJ, Grigsby PL, Haese N, Schabel MC, Wang X et al. Zika virus infection in pregnant rhesus macaques causes placental dysfunction and immunopathology. Nat Commun. 2018; 9:263. https://doi.org/10.1038/s41467-017-02499-9 PMID: 29343712

23. Mohr EL, Block LN, Newman CM, Stewart LM, Koenig M, Semler M et al. Ocular and uteroplacental pathology in a macaque pregnancy with congenital Zika virus infection. PLoS One. 2018; 13:e0190617. https://doi.org/10.1371/journal.pone.0190617 PMID: 29381706

24. Newman CM, Dudley DM, Aliota MT, Weiler AM, Barry GL, Mohns MS et al. Oropharyngeal mucosal transmission of Zika virus in rhesus macaques. Nat Commun. 2017; 8:169. https://doi.org/10.1038/s41467-017-00246-8 PMID: 28765581

25. Dudley DM, Newman CM, Lalli J, Stewart LM, Koenig MR, Weiler AM et al. Infection via mosquito bite alters Zika virus tissue tropism and replication kinetics in rhesus macaques. Nat Commun. 2017; 8:2096. https://doi.org/10.1038/s41467-017-02222-8 PMID: 29235456

26. Haddow AD, Nalca A, Rossi FD, Miller LJ, Wiley MR, Perez-Sautu U et al. High Infection Rates for Adult Macaques after Intravaginal or Intrarectal Inoculation with Zika Virus. Emerg Infect Dis. 2017; 23:1274–1281. https://doi.org/10.3201/eid2308.170036 PMID: 28548637

27. Adams Waldorf KM, Stencel-Baerenwald JE, Kapur RP, Studholme C, Boldenow E, Vornhagen J et al. Fetal brain lesions after subcutaneous inoculation of Zika virus in a pregnant nonhuman primate. Nat Med. 2016; 22:1256–1259. https://doi.org/10.1038/nm.4193 PMID: 27618651

28. Adams Waldorf KM, Nelson BR, Stencel-Baerenwald JE, Studholme C, Kapur RP, Armistead B et al. Congenital Zika virus infection as a silent pathology with loss of neurogenic output in the fetal brain. Nat Med. 2018; 24:368–374. https://doi.org/10.1038/nm.4485 PMID: 29400709

29. Coffey LL, Keesler RI, Pesavento PA, Woolard K, Singapuri A, Watanabe J et al. Intraamniotic Zika virus inoculation of pregnant rhesus macaques produces fetal neurologic disease. Nat Commun. 2018; 9:2414. https://doi.org/10.1038/s41467-018-04777-6 PMID: 29925843

30. Dudley DM, Van Rompay KK, Coffey LL, Ardeshir A, Keesler RI, Bliss-Moreau E et al. Miscarriage and stillbirth following maternal Zika virus infection in nonhuman primates. Nat Med. 2018; 24:1104–1107. https://doi.org/10.1038/s41591-018-0088-5 PMID: 29967348

31. Forsström B, Axnäs BB, Stengele KP, Bühler J, Albert TJ, Richmond TA et al. Proteome-wide epitope mapping of antibodies using ultra-dense peptide arrays. Mol Cell Proteomics. 2014; 13:1585–1597. https://doi.org/10.1074/mcp.M113.033308 PMID: 24705123

32. Zandian A, Forsström B, Häggmark-Månberg A, Schwenk JM, Uhlén M, Nilsson P et al. Whole-Proteome Peptide Microarrays for Profiling Autoantibody Repertoires within Multiple Sclerosis and Narcolepsy. J Proteome Res. 2017; 16:1300–1314. https://doi.org/10.1021/acs.jproteome.6b00916 PMID: 28121444

33. Engmark M, Andersen MR, Laustsen AH, Patel J, Sullivan E, de Masi F et al. High-throughput immunoprofiling of mamba (Dendroaspis) venom toxin epitopes using high-density peptide microarrays. Sci Rep. 2016; 6:36629. https://doi.org/10.1038/srep36629 PMID: 27824133

34. Steffen W, Ko FC, Patel J, Lyamichev V, Albert TJ, Benz J et al. Discovery of a microbial transglutaminase enabling highly site-specific labeling of proteins. J Biol Chem. 2017; 292:15622–15635. https://doi.org/10.1074/jbc.M117.797811 PMID: 28751378

35. Lyamichev VI, Goodrich LE, Sullivan EH, Bannen RM, Benz J, Albert TJ et al. Stepwise Evolution Improves Identification of Diverse Peptides Binding to a Protein Target. Sci Rep. 2017; 7:12116. https://doi.org/10.1038/s41598-017-12440-1 PMID: 28935886

36. Christiansen A, Kringelum JV, Hansen CS, Bøgh KL, Sullivan E, Patel J et al. High-throughput sequencing enhanced phage display enables the identification of patient-specific epitope motifs in serum. Sci Rep. 2015; 5:12913. https://doi.org/10.1038/srep12913 PMID: 26246327

37. Tokarz R, Mishra N, Tagliafierro T, Sameroff S, Caciula A, Chauhan L et al. A multiplex serologic platform for diagnosis of tick-borne diseases. Sci Rep. 2018; 8:3158. https://doi.org/10.1038/s41598-018-21349-2 PMID: 29453420

38. Bailey AL, Buechler CR, Matson DR, Peterson EJ, Brunner KG, Mohns MS et al. Pegivirus avoids immune recognition but does not attenuate acute-phase disease in a macaque model of HIV infection. PLoS Pathog. 2017; 13:e1006692.

39. Aliota MT, Dudley DM, Newman CM, Mohr EL, Gellerup D, Breitbach ME et al. Heterologous Protection against Asian Zika Virus Challenge in Rhesus Macaques. PLoS Negl Trop Dis. 2016; 10:e0005168.

40. Aliota MT, Dudley DM, Newman CM, Weger-Lucarelli J, Stewart LM, Koenig MR et al. Molecularly barcoded Zika virus libraries to probe in vivo evolutionary dynamics. PLoS Pathog. 2018; 14:e1006964.

41. Braack L, Gouveia de Almeida AP, Cornel AJ, Swanepoel R, de Jager C. Mosquito-borne arboviruses of African origin: review of key viruses and vectors. Parasit Vectors. 2018; 11:29. https://doi.org/10.1186/s13071-017-2559-9 PMID: 29316963

42. Pahar B, Kenway-Lynch CS, Marx P, Srivastav SK, LaBranche C, Montefiori DC et al. Breadth and magnitude of antigen-specific antibody responses in the control of plasma viremia in simian immunodeficiency virus infected macaques. Virol J. 2016; 13:200. https://doi.org/10.1186/s12985-016-0652-x PMID: 27903274

43. National Institutes of Allergy and Infectious Diseases. Immune Epitope Database and Analysis Resource; 2018 [cited August 9, 2018]. Database: Immune Epitope Database. Available from: www.iedb.org

44. De Winter J.C.F. Using the Student's t-test with extremely small sample sizes. Practical Assessment, Research & Evaluation 2013; 18:10

45. Lindsey NP, Staples JE, Powell K, Rabe IB, Fischer M, Powers AM et al. Ability To Serologically Confirm Recent Zika Virus Infection in Areas with Varying Past Incidence of Dengue Virus Infection in the United States and U.S. Territories in 2016. J Clin Microbiol. 2018;56

46. Tsai WY, Youn HH, Brites C, Tsai JJ, Tyson J, Pedroso C et al. Distinguishing Secondary Dengue Virus Infection From Zika Virus Infection With Previous Dengue by a Combination of 3 Simple Serological Tests. Clin Infect Dis. 2017; 65:1829–1836. https://doi.org/10.1093/cid/cix672 PMID: 29020159

47. Rönnberg B, Gustafsson Å, Vapalahti O, Emmerich P, Lundkvist Å, Schmidt-Chanasit J et al. Compensating for cross-reactions using avidity and computation in a suspension multiplex immunoassay for serotyping of Zika versus other flavivirus infections. Med Microbiol Immunol. 2017; 206:383–401. https://doi.org/10.1007/s00430-017-0517-y PMID: 28852878

48. Wong SJ, Boyle RH, Demarest VL, Woodmansee AN, Kramer LD, Li H et al. Immunoassay targeting nonstructural protein 5 to differentiate West Nile virus infection from dengue and St. Louis encephalitis virus infections and from flavivirus vaccination. J Clin Microbiol. 2003; 41:4217–4223. https://doi.org/10.1128/JCM.41.9.4217-4223.2003 PMID: 12958248

49. Subissi L, Daudens-Vaysse E, Cassadou S, Ledrans M, Bompard P, Gustave J et al. Revising rates of asymptomatic Zika virus infection based on sentinel surveillance data from French Overseas Territories. Int J Infect Dis. 2017; 65:116–118. https://doi.org/10.1016/j.ijid.2017.10.009 PMID: 29081369

50. Palmeira P, Quinello C, Silveira-Lessa AL, Zago CA, Carneiro-Sampaio M. IgG placental transfer in healthy and pathological pregnancies. Clin Dev Immunol. 2012; 2012:985646. https://doi.org/10.1155/2012/985646 PMID: 22235228

51. Dai L, Song J, Lu X, Deng YQ, Musyoki AM, Cheng H et al. Structures of the Zika Virus Envelope Protein and Its Complex with a Flavivirus Broadly Protective Antibody. Cell Host Microbe. 2016; 19:696–704. https://doi.org/10.1016/j.chom.2016.04.013 PMID: 27158114

52. Barba-Spaeth G, Dejnirattisai W, Rouvinski A, Vaney MC, Medits I, Sharma A et al. Structural basis of potent Zika-dengue virus antibody cross-neutralization. Nature. 2016; 536:48–53. https://doi.org/10.1038/nature18938 PMID: 27338953

53. Ertürk M, Jennings R, Oxley KM, Hastings MJ. Effect of influenza A on phagocytic cell function. Med Microbiol Immunol. 1989; 178:199–209. PMID: 2747589

54. Wang Q, Yang H, Liu X, Dai L, Ma T, Qi J et al. Molecular determinants of human neutralizing antibodies isolated from a patient infected with Zika virus. Sci Transl Med. 2016; 8:369ra179.

55. Zhang S, Kostyuchenko VA, Ng TS, Lim XN, Ooi JS, Lambert S et al. Neutralization mechanism of a highly potent antibody against Zika virus. Nat Commun. 2016; 7:13679. https://doi.org/10.1038/ncomms13679 PMID: 27882950

56. Hasan SS, Miller A, Sapparapu G, Fernandez E, Klose T, Long F et al. A human antibody against Zika virus crosslinks the E protein to prevent infection. Nat Commun. 2017; 8:14722. https://doi.org/10.1038/ncomms14722 PMID: 28300075

57. Robbiani DF, Bozzacco L, Keeffe JR, Khouri R, Olsen PC, Gazumyan A et al. Recurrent Potent Human Neutralizing Antibodies to Zika Virus in Brazil and Mexico. Cell. 2017; 169:597–609.e11. https://doi.org/10.1016/j.cell.2017.04.024 PMID: 28475892

58. Deng YQ, Dai JX, Ji GH, Jiang T, Wang HJ, Yang HO et al. A broadly flavivirus cross-neutralizing monoclonal antibody that recognizes a novel epitope within the fusion loop of E protein. PLoS One. 2011; 6:e16059. https://doi.org/10.1371/journal.pone.0016059 PMID: 21264311